Particle-size effect of nanoscale platinum catalysts in oxygen reduction reaction: an electrochemical and ^{195}Pt EC-NMR study†

Hiroshi Yano,[a] Junji Inukai,[a] Hiroyuki Uchida,[b] Masahiro Watanabe,*[a] Panakkattu K. Babu,[c] Takeshi Kobayashi,[c] Jong Ho Chung,[c] Eric Oldfield*[c] and Andrzej Wieckowski*[c]

Received 24th July 2006, Accepted 15th September 2006
First published as an Advance Article on the web 5th October 2006
DOI: 10.1039/b610573d

Oxygen reduction reaction (ORR) measurements and ^{195}Pt electrochemical nuclear magnetic resonance (EC-NMR) spectroscopy were combined to study a series of carbon-supported platinum nanoparticle electrocatalysts (Pt/CB) with average diameters in the range of roughly 1–5 nm. ORR rate constants and H_2O_2 yields evaluated from hydrodynamic voltammograms did not show any particle size dependency. The apparent activation energy of 37 kJ mol^{-1}, obtained for the ORR rate constant, was identical to that obtained for bulk platinum electrodes. Pt/CB catalysts on Nafion produced only 0.7–1% of H_2O_2, confirming that the direct four-electron reduction of O_2 to H_2O is the predominant reaction. NMR spectral features showed characteristic size dependence, and the line shapes were reproduced by using the layer-deconvolution model. Namely, the variations in the NMR spectra with particle size can be explained as due to the combined effect of the layer-by-layer variation of the *s*-type and *d*-type local density of states. However, the surface peak position of ^{195}Pt NMR spectra and the spin–lattice relaxation time of surface platinum atoms showed practically no change with the particle size variation. We conclude that there is a negligible difference in the surface electronic properties of these Pt/CB catalysts due to size variations and therefore, the ORR activities are not affected by the differences in the particle size.

1. Introduction

Investigations of the electronic properties of transition metal nanoparticles and correlating them with their catalytic activities is a central theme in heterogeneous catalysis.[1] Among the transition metals, platinum possesses some well-known properties that make it a special catalyst with potential applications in a wide range of chemical reactions, including fuel cells. Carbon-supported platinum nanoparticles (Pt/CB, where CB = carbon black) can be used as catalysts for both the anode as well as the cathode of polymer electrolyte fuel cells (PEFCs).

In order to obtain high mass activity of platinum in fuel cells, it is essential to disperse platinum nanoparticles on high surface area supports. Bregoli stated that as the specific surface area of Pt (S_{Pt}°) on CB increased from 20 to 80 m^2 g^{-1} (corresponding to particle diameter d_{Pt} of *ca.* 14 nm to 3.5 nm) the specific activity towards the oxygen reduction reaction (ORR) decreased.[2] Ross and coworkers extended this work to higher surface area platinum and observed a similar but more pronounced effect in the region of S_{Pt}° greater than 80 m^2 g^{-1} with $d_{Pt} < 3$ nm.[3,4] Both studies suggested that the particle-size effect might be attributed to morphological changes of the particles, *e.g.* the relative concentration of surface atoms of different coordination number or the ratio of preferable crystal planes on the crystalline surface.[5] Takasu *et al.* also reported lower activities on smaller platinum particles in the ORR and in the oxidation of small organic molecules. They attributed the particle-size effect to larger adsorption energies due to the change in the electronic structure of smaller particles.[6] Mukerjee and McBreen carried out *in situ* X-ray absorption spectroscopy measurements and reported changes in the electronic structure in an electrolyte solution.[7] Durand and coworkers examined the ORR on Pt/CB catalysts in a sulfuric acid solution at room temperature and confirmed similar particle-size effects.[8] Watanabe *et al.* investigated the platinum particle-size effect on the ORR in both hot phosphoric and sulfuric acid solutions.[9,10] It was found that when the average inter-particle distance was larger than *ca.* 20 nm, the catalyst (apparent) specific activity was fully utilized, *i.e.*, the reaction rate was independent of the platinum particle size. (However it did depend on the inter-particle distance.) Therefore, the particle-size effect reported previously was not confirmed.[9,10] Further, Watanabe *et al.* examined the process of electro-oxidation of methanol on Pt/CB in sulfuric acid media, and found no particle-size effect even down to d_{Pt} as small as

[a] *Interdisciplinary Graduate School of Medicine and Engineering, University of Yamanashi, Clean Energy Research Center, Takeda 4, Kofu, 400-8511, Japan. E-mail: m-watanabe@yamanashi.ac.jp*
[b] *Interdisciplinary Graduate School of Medicine and Engineering, Takeda 4, Kofu, 400-8511, Japan*
[c] *University of Illinois at Urbana-Champaign, Department of Chemistry, 600 South Mathews, Urbana, Illinois, 61801, USA. E-mail: andrzej@scs.uiuc.edu; eo@chad.scs.uiuc.edu*
† Electronic supplementary information (ESI) available: XRD patterns. See DOI: 10.1039/b610573d

1.4 nm.[11] It is also noted that the particle-size effect on H_2O_2 production yield is still unclear, although H_2O_2 may deteriorate the polymer electrolyte membrane or gaskets. In order to resolve these controversies and elucidate any real particle size effect, a combined electrochemical and spectroscopic investigation was essential, and therefore, we carried out ORR activity measurements and electrochemical nuclear magnetic resonance (EC-NMR) on these Pt/CB catalysts. The results of this combined approach are reported here.

EC-NMR experiments have proven to be very useful in correlating the surface electronic properties of anodes with their catalytic activities in methanol oxidation reactions.[12–16] For instance, bimetallic catalysts with improved CO tolerance, prepared by surface modification of Pt-black *via* spontaneous deposition of Ru, showed a direct correlation between the methanol oxidation current densities and the Fermi level local density of states (E_f-LDOS) of surface Pt atoms,[17] whereas the ^{195}Pt NMR studies of Pt–Ru alloy nanoparticles revealed the surface segregation of platinum and the effect of heat-treatment in improving the catalytic activity towards methanol oxidation.[13,18] The NMR spectra of metal nanoparticles reflect the distribution in E_f-LDOS across the nanoparticles,[19–23] and the spin–lattice relaxation (T_1) behavior is very effective for studying the interaction between adsorbates and metal surfaces, and also the motional aspects of adsorbates.[21,24,25] For metallic systems, the shift in the NMR spectrum (Knight shift, K) and the spin–lattice relaxation time (T_1) are determined by the electron-nucleus hyperfine interactions.[26] The ability to provide detailed information about the surface electronic states of nanoparticles is a large advantage of EC-NMR. Therefore, the application of ^{195}Pt NMR to cathode catalysts is a both interesting and promising approach.

In the present research, as a joint effort, we performed electrochemical ORR and ^{195}Pt EC-NMR measurements for Pt/CB catalysts with three batches of Pt nanoparticles of diameters d_{Pt} 1.6 ± 0.4, 2.6 ± 0.7, and 4.8 ± 1.0 nm (see Experimental section). An apparent ORR rate constant (k_{app}) and the activation energy (E_a) were determined using a channel flow double electrode (abbreviated below as CFDE) cell[27–29] operated as a closed system with controlled oxygen concentration and at elevated temperatures. We quantified both ORR kinetics and the H_2O_2 production rate using a collecting electrode located at the downstream of the working electrode in the CFDE. For the same set of Pt/CB electrocatalysts, we carried out low temperature ^{195}Pt NMR measurements. The particle-size effect of platinum towards ORR is discussed based upon the electrochemical and NMR analyses.

2. Experimental

In the present investigation, we used three Pt/CB electrocatalysts (d_{Pt} = 1.6, 2.6, and 4.8 nm) provided by Tanaka Kikinzoku Kogyo, for which X-ray diffraction measurements were carried out using a Rigaku RINT2000 spectrometer with Cu Kα radiation (1.54 nm, 50 kV, 300 mA). Details of the experimental set-up for the ORR measurements using the CFDE cell and flow circuit of electrolyte solution are described in the literature.[27–29] The working electrode consisted of Pt/CB catalysts perfectly dispersed on a Au substrate electrode (flow direction length 1 mm × width 4 mm) at a constant loading of carbon support, 5.45 μg cm^{-2}, which corresponds to approximately a monolayer height of the carbon black particles.[29,30] 0.2 wt% Nafion diluted with a mixed solution of ethanol and water (3 : 2 in vol.%) was put on top of the catalyst layer to yield the average film thickness of 0.1 μm. The Nafion-coated electrode was dried under ethanol vapor pressure at room temperature. Finally, Nafion–Pt/CB on gold was heated at 130 °C for 30 min in air.

The platinum collecting electrode (1 × 4 mm) was used to detect H_2O_2. A platinum wire was used as the counter electrode. A reversible hydrogen electrode RHE(t) kept at the same temperature as that of the cell was used as the reference electrode. The electrolyte solution of 0.1 M $HClO_4$ was prepared from reagent grade chemicals (Kanto Chemical Co.) and Milli-Q water, and purified in advance with conventional pre-electrolysis methods. The electrolyte solution was saturated with O_2 or N_2 gas bubbling for at least 1 h prior to the electrochemical measurements. A bi-potentiostat (ALS 700B, BAS Inc.) was used for the CFDE measurements. Hydrodynamic voltammograms at the working electrode under a flow of O_2-saturated 0.1 M $HClO_4$ solution (mean flow rate = 10–50 cm s^{-1}) were recorded by scanning the potential from 0.3 to 1.5 V *vs.* RHE(*t*) at 0.5 mV s^{-1}. The potential of the collecting electrode was set at 1.2 V where H_2O_2 was oxidized under a diffusion control condition. The collection efficiency of the present CFDE system was experimentally determined to be 0.28 ± 0.01. During heating or cooling to a desired temperature, the potential for the working electrode was kept at 1.0 V.

Average particle diameters and size distributions were studied by transmission electron microscopy (TEM) using a JEOL 2010F instrument. The Tanaka Pt/CB catalysts were dispersed in about 2 ml of Millipore water and sonicated. The suspension was dropped onto holy carbon grids and dried before the TEM measurements.

For the NMR measurements, each sample was electrochemically cleaned to remove the surface oxides[31] by holding the potential at 0.46 V (*vs.* RHE) under a continuous stream of ultrapure Ar in a three electrode electrochemical cell, containing a platinum wire gauze as counter electrode, a Ag|AgCl|3 M NaCl reference electrode and the working electrode made of about 300 mg of the as-received Pt/CB catalyst particles contained within a platinum boat. The cell potential was controlled by a potentiostat (AUTOLAB, Ecochemie, Netherlands). 0.5 M H_2SO_4 with D_2O (99% enriched, SIGMA-Aldrich) used as the electrolyte. After the electrochemical treatment, the sample was transferred, together with a small portion of the electrolyte, into an NMR ampoule (10 mm in diameter, 25 mm in length) and then flame sealed. ^{195}Pt NMR spectra were obtained ''point-by-point'' by recording the spin-echo intensities as a function of applied radio frequency (from 74 to 78 MHz in steps of 0.1 MHz) using a ''home-built'' NMR spectrometer operated in the field of a superconducting solenoid magnet (8.47 T, Oxford Instruments, UK). The 90° pulse width of 5 μs and a τ value of 30 μs were used. Spin–lattice relaxation time (T_1) measurements were made using a saturation comb of 20 pulses followed by a spin echo sequence for detection. All ^{195}Pt NMR measurements were

carried out using an NMR probe housed in a continuous He-flow cryostat (CF1200, Oxford Instruments, MA). Field/frequency ratios for ^{195}Pt are reported with respect to the resonance of H_2PtI_6.

3. Results and discussion

3.1 ORR catalytic activity measurements

Fig. 1 shows the hydrodynamic voltammograms for the ORR at the Nafion–Pt/CB working electrode prepared from the 1.6 nm size catalyst in 0.1 M $HClO_4$ solution saturated with O_2 and the currents simultaneously acquired at a platinum collecting electrode at 30 °C. The flow rate of solution was varied from 10 to 50 cm s^{-1}, and the currents at both working and collecting electrodes were found to increase with increasing flow rate. Fig. 2 shows the hydrodynamic voltammograms for ORR at three different catalysts (1.6, 2.6, and 4.8 nm) obtained at 30 °C under a solution flow rate of 50 cm s^{-1}. For comparison, the hydrodynamic voltammograms at Nafion–Pt(bulk) and Nafion–Pt/CB prepared with 2.6 nm size catalyst with 19.3 wt% platinum loading (the same platinum loading as the 1.6 nm catalyst) are also shown. The ORR currents at the working electrode commenced at *ca.* 0.95 V and reached the diffusion limits at around 0.5 V.

Based on the collection efficiency, N, at the collecting electrode, we calculated the ratio of H_2O_2 formation rate to the overall ORR rate, $P(H_2O_2)$, using

$$P(H_2O_2) = 2I_c/(N \times I_w + I_c) \times 100\% , \qquad (1)$$

where I_w and I_c are the currents at the working and collecting electrodes, respectively. We found that Nafion-coated carbon black (without platinum) and Au substrate produced H_2O_2 with $P(H_2O_2)$ = 98% only in the less positive potential region, $E < 0.65$ V, but the H_2O_2 production at $E > 0.7$ V was thoroughly ascribed to Nafion–Pt/CB.[29] As seen in Fig. 3, the values of $P(H_2O_2)$ at Nafion–Pt/CB are almost the same as those at Nafion–Pt(bulk) within an experimental error for all the catalysts, irrespective of platinum particle size and platinum loading. The $P(H_2O_2)$ increases slightly with lowering the potential, *i.e.*, 0.6, 0.7, and 1.0% at 0.80, 0.76, and 0.70 V, respectively, and is almost independent of the temperature from 50 to 110 °C. Because the $P(H_2O_2)$ was zero at Pt(bulk) (without Nafion),[27,28] the Nafion coating on platinum is the major cause for triggering the H_2O_2 production at a practical potential region for PEFCs, $E > 0.70$ V. It has been reported that the hydrogen adsorption/desorption charge at the Nafion–Pt(bulk) decreases by about 10% compared with the Pt(bulk) (without Nafion) electrode.[29,32–35] This reduction is probably due to a specific adsorption of sulfonate groups in Nafion, as observed by *in situ* infrared spectroscopy.[36] In this study, therefore, sulfonate groups in Nafion could be the possible species strongly adsorbed on platinum surface, modifying the surface property.[19]

Here, we discuss the effect of Pt particle size on the ORR rate constant. The kinetically controlled current I_k at a given potential E is determined from the hydrodynamic voltammogram in the CFDE by using the following equation.

$$1/I = 1/I_k + 1/I_L = 1/I_k + 1/\{1.165 \times nF[O_2]w(U_m D^2 x_1^2/h)^{1/3}\} \qquad (2)$$

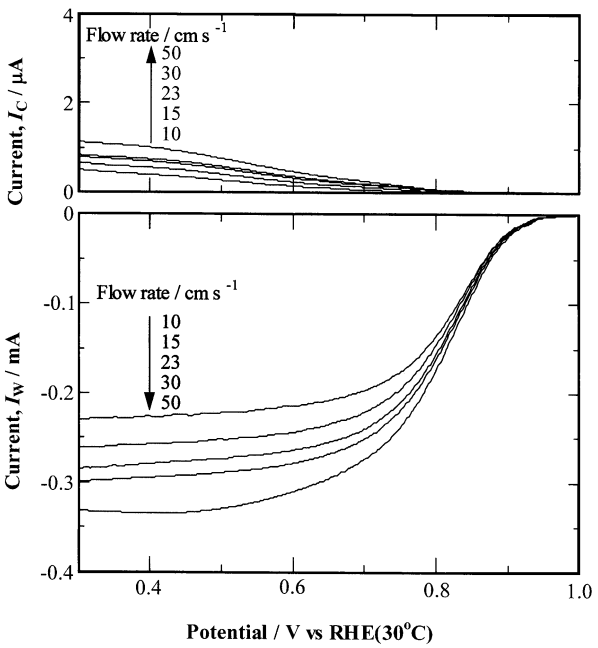

Fig. 1 Hydrodynamic voltammograms for the ORR at Nafion-coated 1.6 nm Pt/CB working electrode in an O_2-saturated 0.1 M $HClO_4$ solution and simultaneously acquired current at a Pt collecting electrode (E = 1.2 V) at 30 °C. Potential sweep rate = 0.5 mV s^{-1}.

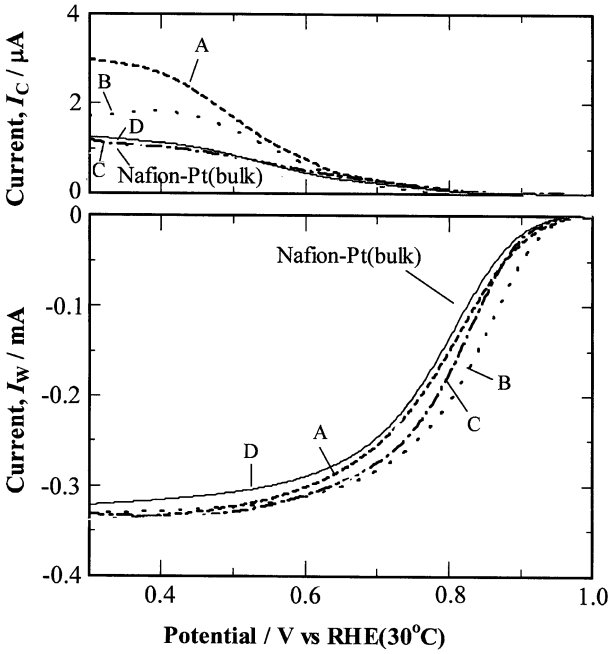

Fig. 2 Hydrodynamic voltammograms for the ORR at Nafion–Pt(4.8 nm)/CB (curve A), Nafion–Pt(2.6 nm)/CB (curve B), Nafion–Pt(1.6 nm)/CB (curve C), Nafion–Pt(2.6 nm)/CB with the same Pt loading as 1.6 nm size catalyst (curve D), and Nafion–Pt(bulk) electrodes in O_2 saturated 0.1 M $HClO_4$ solution and simultaneously acquired current at a Pt collecting electrode at 30 °C. Electrolyte solution flow rate U_m = 50 cm s^{-1}. Potential sweep rate = 0.5 mV s^{-1}.

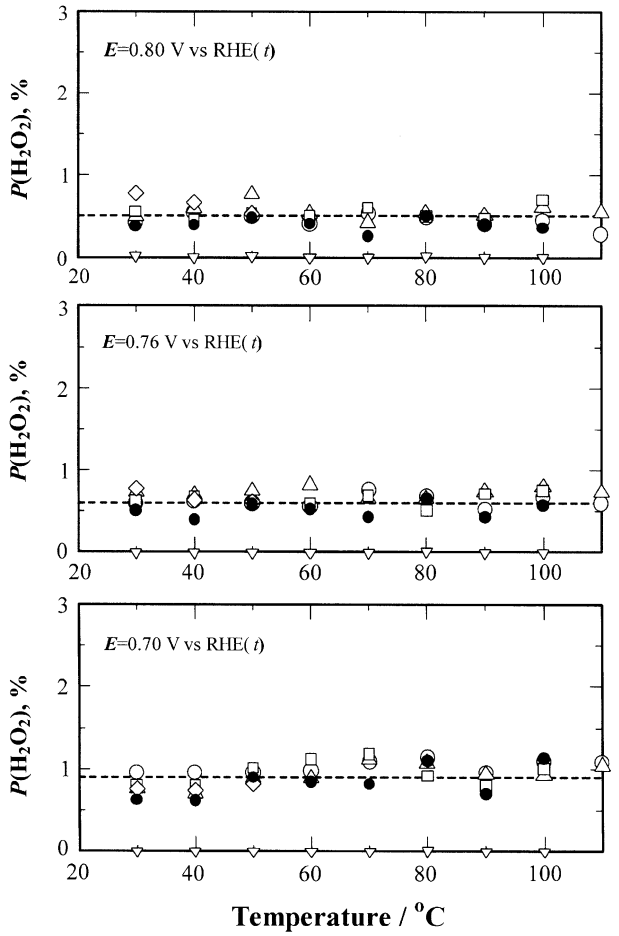

Fig. 3 Temperature dependence of H_2O_2 yield $P(H_2O_2)$ at (○) Nafion–Pt(4.8 nm)/CB, (Δ) Nafion–Pt(2.6 nm)/CB, (◇) Nafion–Pt(1.6 nm)/CB, (□) Nafion–Pt(2.6 nm)/CB with the same Pt loading as 1.6 nm size catalyst, (●) Nafion–Pt(bulk), and (▽) Pt(bulk) without Nafion coating. U_m = 50 cm s^{-1}. Data on (◇) at high temperatures (>50 °C) were omitted.

where n is the number of electrons transferred, F is the Faraday constant, $[O_2]$ is the O_2 concentration in the bulk of electrolyte solution, w is the width of the working electrode, U_m is the mean flow rate of the electrolyte solution, D is the diffusion coefficient of O_2, x_1 is the length of the working electrode in the electrolyte flow direction, and h is the half channel height (or the half thickness of the electrolyte flow over the electrodes). An example of I^{-1} *vs.* $U_m^{-1/3}$ plots for ORR on 1.6 nm Pt/CB catalyst is shown in Fig. 4, obtained from hydrodynamic voltammograms in O_2 saturated 0.1 M $HClO_4$ solution at 30 °C. A linear relationship was seen between I^{-1} and $U_m^{-1/3}$ on all of the Pt/CB samples and at all the potentials of 0.80, 0.76, and 0.70 V examined. By extrapolating $U_m^{-1/3}$ to 0 (infinite flow rate), the value of I_k can be calculated. However, the value of I_k is not a suitable measure of the ORR activity because the I_k values depend not only on the active Pt surface area (S_{Pt}) of each sample but also on the $[O_2]$ in the electrolyte solution, which decreases with elevating temperatures. Details of the estimation of the $[O_2]$ at different temperatures were described in our previous paper.[27] Since the contribution of two-electron reduction to produce

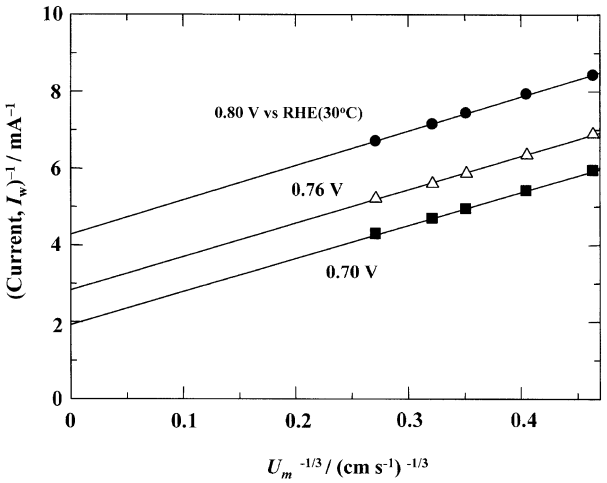

Fig. 4 An example of I^{-1} *vs.* $U_m^{-1/3}$ relationship, so-called Levich–Koutecky plots, for the ORR on Nafion–Pt (1.6 nm)/CB catalyst at 30 °C, obtained from hydrodynamic voltammograms in O_2 saturated 0.1 M $HClO_4$ solution.

H_2O_2 (to the overall ORR) was very low (see Fig. 3), we can evaluate an apparent rate constant k_{app} at a constant applied potential similar to our previous work[27–29] from the eqn (3),

$$I_k/(4\,FS_{Pt}) = -k_{app}[H^+][O_2] \qquad (3)$$

where $[H^+]$ is the bulk concentration of H^+ (0.1 M) and S_{Pt} is the electrochemically active surface area obtained from the cyclic voltammograms measured at 30 °C, as shown in Fig. 5. We always checked the value of S_{Pt} at 30 °C after the ORR measurement at a given temperature (30–110 °C). It was found that the values of S_{Pt} of 4.6 nm size and 2.6 nm size catalysts were unchanged even after the measurement at 110 °C. While the S_{Pt} at the 1.6 nm size catalyst was almost constant after the measurement at 50 °C, it decreased significantly once heated at a temperature higher than 60 °C (Fig. 5B). It was found by TEM that the platinum particles had grown to *ca.* 1.9 nm from the original size of 1.6 nm. Hence, we will demonstrate the ORR properties of the 1.6 nm catalyst at 30–50 °C, because the effect of particle-size on the stability is out of scope in the present research.

Arrhenius plots of the apparent rate constants k_{app} for the different Nafion–Pt/CB electrodes are shown in Fig. 6. Because both E° and E[RHE(t)] shift to less positive values in different manners, the corrected potential, E, is applied so as to keep a constant applied potential, (E–E°), for the ORR at each temperature.[27] Linear relationships between the log k_{app} and $1/T$ are observed at all the electrodes in the whole temperature range. Each solid line is the least square fitting of all the data at the constant applied potential. From the slope, we obtained an apparent activation energy of E_a = 37 kJ mol^{-1} at −0.525 V *vs.* E°, which is in very good agreement with the earlier reported value for bulk platinum electrodes.[27] The values of k_{app} at Nafion–Pt/CB with different platinum particle sizes beautifully agreed with those at Nafion–Pt(bulk) in the whole temperature range and at practical potential range. Hence, the ORR rate constant and its activation energy

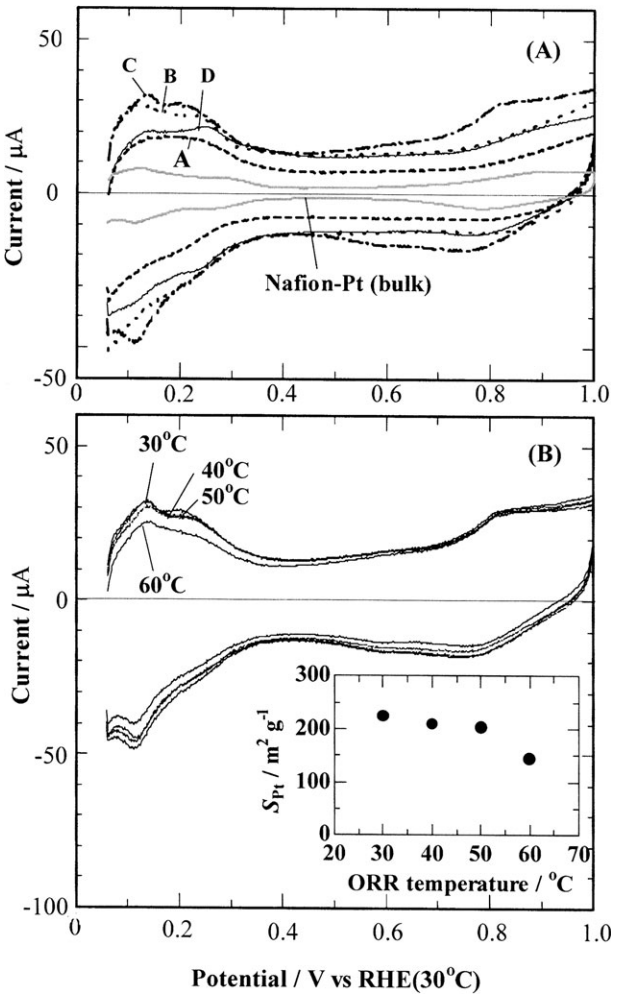

Fig. 5 (A) Cyclic voltammograms to determine the electrochemical active area S_{Pt} at Nafion–Pt(4.8 nm)/CB (curve A), Nafion–Pt(2.6 nm)/CB (curve B), Nafion–Pt(1.6 nm)/CB (curve C), Nafion–Pt(2.6 nm)/CB with the same Pt loading as 1.6 nm size catalyst (curve D), and Nafion–Pt(bulk) electrodes in N_2 saturated 0.1 M $HClO_4$ solution at 30 °C. Potential sweep rate = 0.1 V s^{-1}. (B) Temperature dependency of the cyclic voltammograms of Nafion–Pt(1.6 nm)/CB catalyst in 0.1 M $HClO_4$ solution saturated with N_2. Potential sweep rate = 0.1 V s^{-1}. Inset shows the changes in the specific surface area of 1.6 nm Pt/CB catalyst after the ORR measurements at various temperatures.

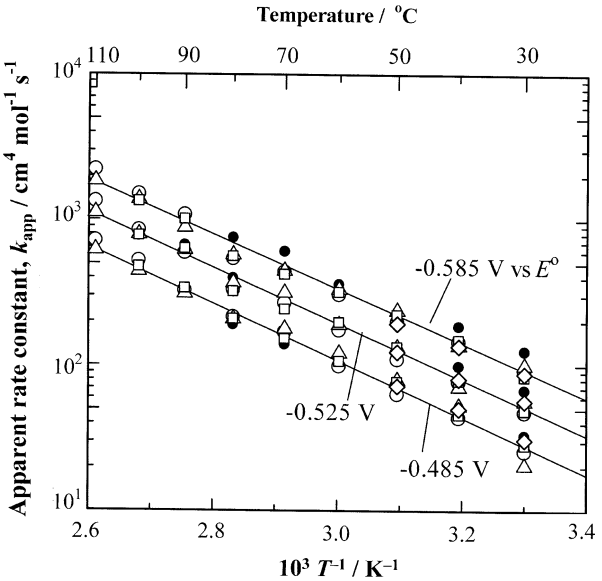

Fig. 6 Arrhenius plots of the ORR rate constants k_{app} obtained for (○) Nafion–Pt(4.8 nm)/CB, (△) Nafion–Pt(2.6 nm)/CB, (◇) Nafion–Pt(1.6 nm)/CB, (□) Nafion–Pt(2.6 nm)/CB with the same Pt loading as 1.6 nm size catalyst, and (●) Nafion–Pt(bulk). Data on (◇) at high temperatures (>50 °C) were omitted. Each solid line is the least square fitting of all the data at the constant applied potential. The applied potential of −0.485, −0.525, and −0.585 V *vs.* E° corresponds to 0.80, 0.76, and 0.70 V *vs.* RHE at 30 °C, respectively.

are independent of the platinum particle size. Because both the ORR activity per real platinum active surface area and the $P(H_2O_2)$ are the same, we can reduce the mass of platinum in the catalyst layer by using the smaller size particles as long as their durability can be confirmed.

Ross and coworkers reported the ORR activity on single crystal Pt surfaces using the rotating ring-disk electrode technique in various electrolyte solutions.[37] While the ORR activities increased in the order Pt(111) < Pt(100) < Pt(110) in 0.05 M H_2SO_4 probably due to the decrease in the adsorption of bisulfate anions, the variation in the activities was relatively small among the three low index crystal facets in 0.1 M $HClO_4$ of a weakly-adsorbed anion. In the present research, the ORR activities (k_{app}) of Pt/CB coated with specifically adsorbed Nafion in 0.1 M $HClO_4$ solution are not affected by the differences in the particle size. By XRD measurements, diffraction peaks from (111), (200), (220), and (311) planes were observed on all nanoparticle catalysts, and the peak ratios were almost the same in their XRD patterns. This suggests that the relative ratio of facets exposed on the Pt nanoparticles was certainly unchanged among the Pt/CB catalysts with Pt particle sizes from 1 to 5 nm. This identical relative ratio of facets explains the same reaction rate towards the ORR on Pt/CB coated with Nafion specifically adsorbed on Pt nanoparticles.

3.2 TEM measurements

Fig. 7 shows the histograms of particle size distributions obtained by the TEM measurements. Each histogram is constructed from diameters measured for 650 ~ 850 counts of nanoparticles. The average diameters with standard deviations and dispersions are summarized in Table 1. It is evident that these three catalysts have narrow size distributions and are ideal to probe the Pt nanoparticle size effects. Assuming that the particles have an ideal cubooctahedral shape, we can determine the total number of atoms (N_T), the number of layers (l) and the number of surface atoms for a particle with diameter d from the following equations.[21]

$$N_T = \frac{2\pi}{3}\left(\frac{d_{Pt}}{a}\right)^3 \quad (4)$$

$$N_T = \frac{10}{3}l^3 - 5l^2 + \frac{11}{3}l - 1 \quad (5)$$

$$N_S = 10l^2 - 20l + 12 \quad (6)$$

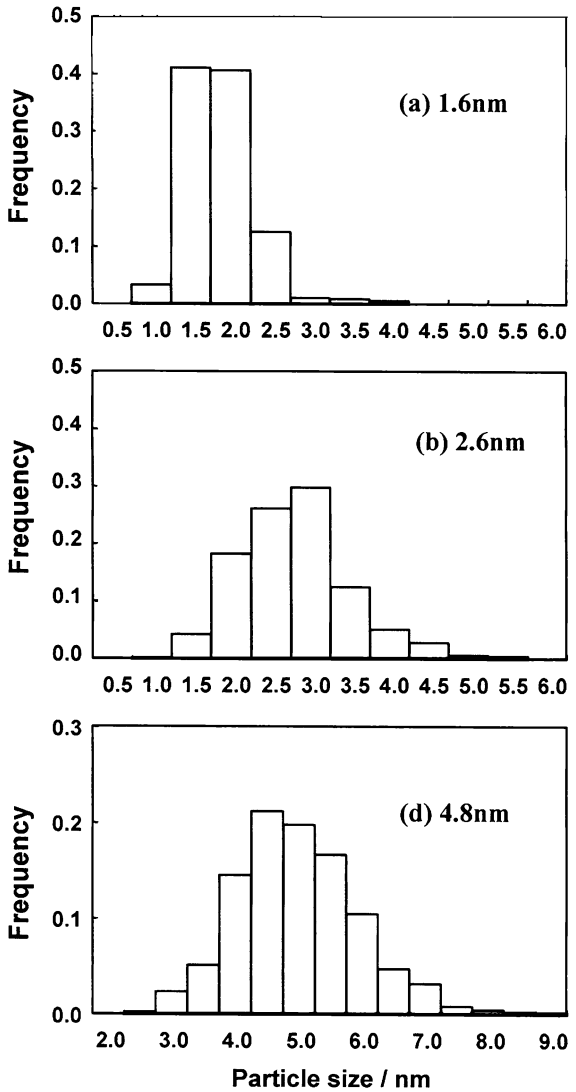

Fig. 7 Particle size distributions obtained from TEM, for the three Pt/CB catalysts. The average particle sizes are (a) 1.6, (b) 2.6, and (c) 4.8 nm.

Here, d_{Pt} is the mean diameter of platinum particles determined based on TEM data shown in Fig. 7, and a is the lattice parameter and equals 0.392 nm for platinum. Fig. 8 shows the layer statistics for the three catalysts, calculated with the above equations. For the 1.6 nm catalyst, more than 50% of the atoms reside on the surface layer whereas for the 4.8 nm catalyst, only 25% of atoms are on the surface of the nanoparticle.

Table 1 Particle size variation of dispersion, Pt loading (wt%-Pt in Pt/CB), Knight shift healing length and spin–lattice relaxation time at the surface peak

Pt size d_{Pt}/nm	Dispersion (%)	Pt loading (wt%)	Healing length (layers)	T_1 measured at the surface peak/ms
1.6 ± 0.4	55	19.4	3.7 ± 0.2	2.6 ± 0.5
2.6 ± 0.7	39	46.7	3.1 ± 0.1	2.4 ± 0.4
4.8 ± 1.0	24	50.4	1.8 ± 0.1	1.7 ± 0.3

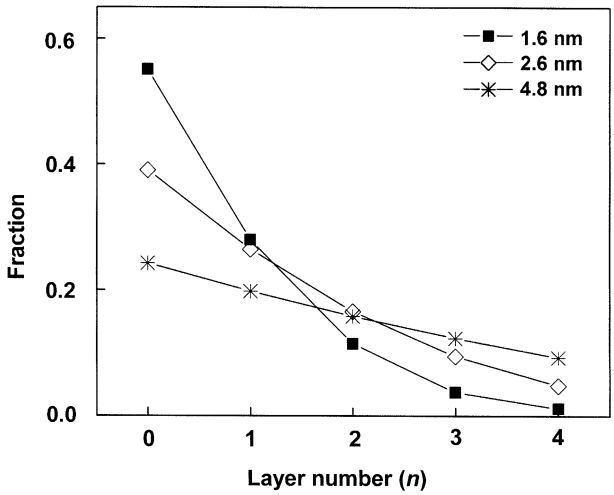

Fig. 8 Fraction of atoms over different atomic layers (layer statistics) calculated by assuming cubooctahedral geometry. (Layer numbers 0 and 1 are the surface and the subsurface layer, respectively).

3.3 ^{195}Pt NMR measurements

Now that the ORR activity by electrochemical measurements and the particle-size distribution by TEM were obtained, we carried out the NMR spectroscopic measurements with these (the same as above) catalyst samples. The ^{195}Pt NMR spectra of the electrochemically cleaned Pt/CB catalysts at 10 K are shown in Fig. 9. The y-axis data are normalized to the maximum spin echo intensity. These platinum catalysts give rise to the spin echo intensities ranging from the field/frequency ratio of 1.085 to 1.145 G kHz^{-1}. Earlier investigations have identified that the signal at the field/frequency ratio of 1.100 G kHz^{-1} corresponds to the surface atoms of platinum nanoparticles while the ^{195}Pt NMR spectrum of atoms in the inside layers of a nanoparticle gives rise to NMR responses toward the bulk platinum (metal) NMR peak, which appears at 1.138 G kHz^{-1}.[24,31] Fig. 9 shows that the surface signal is enhanced for small particles due to the large fraction of surface atoms, whereas for the larger particles, NMR response near 1.138 G kHz^{-1} is enhanced due to the larger fraction of atoms in the inside layers. For the two smaller sets of particles (1.6 and 2.6 nm) there is very little or no NMR response near 1.138 G kHz^{-1} indicating that the fraction of platinum atoms with electronic environment similar to that of bulk platinum is negligibly small. For the larger diameter particles (4.8 nm), a significant fraction of platinum atoms have attained an electronic environment identical to that of bulk platinum and therefore, we can see a large NMR intensity near the 1.138 G kHz^{-1} region.

The variation in the NMR line shape with particle size can be interpreted as due to the combined effect of the layer-by-layer variation of s and d-like E_f-LDOS. The resonance frequency for a given platinum atom in an average nanoparticle is determined by the sum of the positive s-like and the negative d-like hyperfine fields at the nucleus.[38] In bulk platinum, the d-like hyperfine field provides the dominant contribution to the Knight shift. Moving from the core of the particle to the surface, the d-electron E_f-LDOS

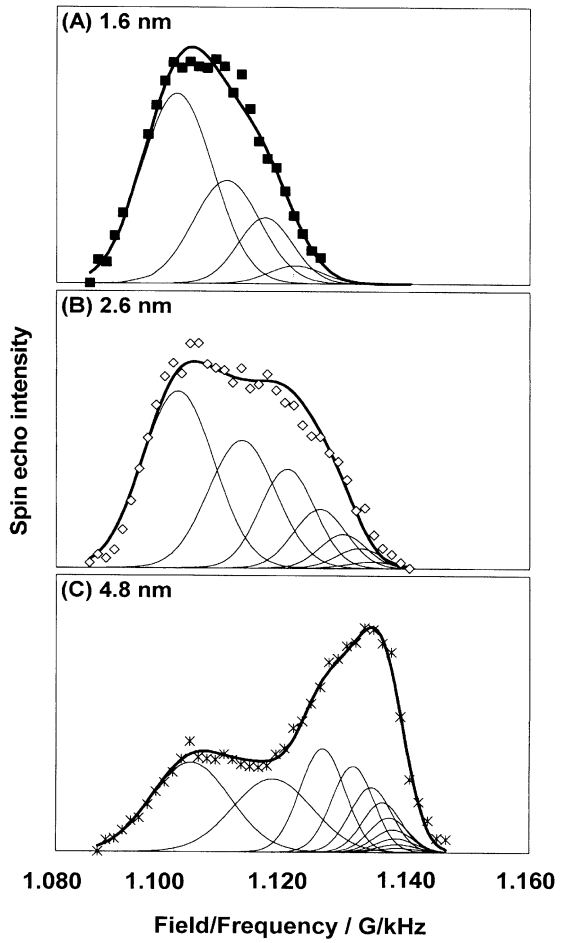

Fig. 9 ^{195}Pt NMR spectra and the layer-model deconvolution. Symbols represent the experimentally obtained spin echo intensities, and the thick solid lines correspond to the convolution pattern obtained from the Gaussian peaks (thin solid lines). Each Gaussian represents the NMR signal of nuclei in a given layer. The area of each Gaussian is taken to be proportional to the population by the layer statistics shown in Fig. 8.

monotonously decreases[39,40] and the Knight shift decreases as well.[41–44]

In the layer model analysis of ^{195}Pt NMR spectra,[21,22] the particles are assumed to be made of several layers of platinum atoms in a cubo-octahedral geometry. The NMR response from a given layer is assumed to be a Gaussian whose peak represents the average Knight shift of that layer. If the particle size distribution of the sample is known, the experimentally obtained NMR spectrum can be represented by a convolution of those Gaussian peaks. The center of the Gaussian, that is the Knight shift of the platinum atom layer, heals back exponentially toward the bulk platinum position according to the following equation when moving from the surface to the center of a particle.

$$K_n = K_\infty + (K_0 - K_\infty)\exp(-l/m_l) \qquad (4)$$

Here, l is the layer number, counting inward from the surface layer ($l = 0$), m_l is the characteristic number of layers defining

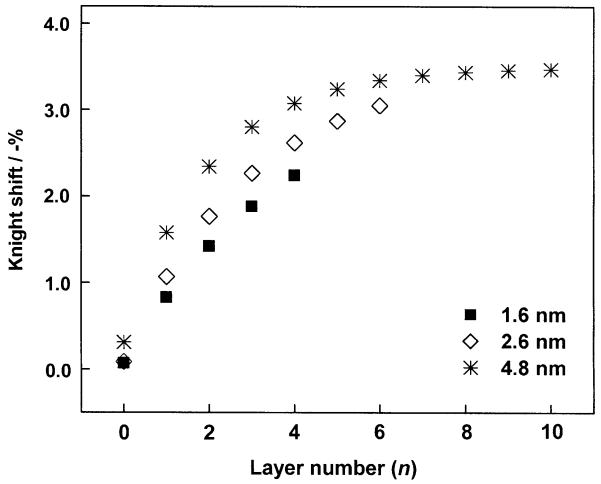

Fig. 10 Layer to layer variation of the Knight shift and its particle size dependence.

the "healing length" for the Knight shift. K_0 and K_∞ are the Knight shifts of the surface layer and bulk platinum, respectively ($K_\infty = -3.49\%$ for H_2PtI_6 as reference). The NMR spectra are deconvoluted by taking the individual Gaussian intensities to be proportional to the layer statistics of atoms in each layer.

Assuming a cubo-octahedral model, the 1.6, 2.6 and 4.8 nm particles have 4, 6, and 11 layers, respectively. The deconvoluted spectra based on the layer model are also shown in Fig. 9 and are in good agreement with the experimental results. The healing lengths obtained from the deconvolution are given in Table 1 and variations in the Knight shift at each layer are shown in Fig. 10.

It is most important to notice that although the Knight shift for the interior layers shows particle size dependence, the surface Knight shifts show no noticeable size dependence (Fig. 9 and 10), where all Knight shifts are nearly 0%. This implies that the electronic nature of surface platinum atoms is identical in all of the three samples. In our study, using the electrochemical measurements and the CFDE cell, no particle-size effect was observed on ORR, as shown above. Therefore, we conclude that the identical electronic structure at surfaces of different platinum nanoparticles explains the similar reaction rates at all platinum surfaces towards the ORR. This observation is further confirmed by the T_1 measurements. Spin–lattice relaxation times (T_1) measured at the surface position (1.104 G kHz^{-1}) at 10 K are shown in Table 1. Within the limits of the experimental error, measured value of T_1 is equal to $\sim$2 ms for all the three samples. Again, this observation has important implications for the catalytic activity of these nanoparticles. In the case of metallic substances, the conduction electrons causing the Knight shift are responsible for the T_1 relaxation rate due to energy exchange between nuclear spins and the conduction electron states lying very close to the Fermi level.[41] Since the Knight shift and T_1 of surface Pt atoms are nearly identical, we can conclude that the E_f-LDOS of surface Pt atoms do not vary with particle size. Therefore, the surface electronic state is the same on the three catalysts investigated in this report, which also explains the close similarity of their ORR activities.

In order to achieve a higher mass activity of platinum, smaller nanoparticles in size are preferable as understood by our electrochemical measurements: fabricating stable Pt cluster catalysts is a next step to be studied. By EC-NMR, an identical electronic nature of surface platinum atoms in samples with different sizes was implied. The investigation on additives to platinum could find a promising route to modify both the electronic nature and stability of catalysts.[1]

4. Conclusions

We measured the ORR activities on a series of carbon-supported platinum nanoparticles of various average particle diameters. The same set of Pt/CB catalysts was investigated by ^{195}Pt EC-NMR. It was found that the apparent ORR rate constants and the activation energies were independent of the particle size, and were identical to those for bulk platinum electrodes. The H_2O_2 yields were also identical to those for the Nafion-coated bulk platinum electrode. By ^{195}Pt NMR, the surface peak positions and relaxation rates showed only marginal variations with the particle size indicating that the E_f-LDOS of surface platinum atoms are identical. By combining the NMR results with the ORR measurements, we conclude that the electronic properties of the surface atoms on platinum nanoparticles do not show any particle size effect and therefore, their ORR activities are also particle size independent.

Acknowledgements

This research was supported by a grant from the US National Science Foundation (CTS-02-12216). A part of this research was supported by the fund for "Leading Project" of Ministry of Education, Science, Culture, Sports and Technology of Japan. The authors would also like to thank Tanaka-Kikinzoku Co. for providing the catalysts.

References

1 *Catalysis and Electrocatalysis at Nanoparticle Surface*, ed. A. Wieckowski, E. R. Savinova and C. G. Vayenas, Marcel Dekker, New York, 2003.
2 L. J. Bregoli, *Electrochim. Acta*, 1978, **23**, 489.
3 P. N. Ross, in *Precious Metals 1986*, ed. U. V. Rao, International Precious Metals Institute, Allentown, PA, 1986, p. 355.
4 M. L. Sattler and P. N. Ross, *Ultramicroscopy*, 1986, **20**, 21.
5 K. Kinoshita, *J. Electrochem. Soc.*, 1990, **137**, 845.
6 Y. Takasu, N. Ohashi, X.-G. Zhang, Y. Murakami and K. Yahikozawa, *Electrochim. Acta*, 1996, **41**, 2595.
7 S. Mukerjee and J. McBreen, *J. Electroanal. Chem.*, 1989, **448**, 163.
8 A. Kabbabi, F. Gloaguen, F. Andolfatto and R. Durand, *J. Electroanal. Chem.*, 1994, **373**, 251.
9 M. Watanabe, S. Saegusa and P. Stonehart, *Chem. Lett.*, 1988, 1487.
10 M. Watanabe, H. Sei and P. Stonehart, *J. Electroanal. Chem.*, 1989, **261**, 375.
11 M. Watanabe, S. Saegusa and P. Stonehart, *J. Electroanal. Chem.*, 1989, **271**, 213.
12 Y. Y. Tong, H. S. Kim, P. K. Babu, P. Waszczuk, A. Wieckowski and E. Oldfield, *J. Am. Chem. Soc.*, 2002, **124**, 468.
13 P. K. Babu, H. S. Kim, S. T. Kuk, J. H. Chung, E. Oldfield, A. Wieckowski and E. S. Smotkin, *J. Phys. Chem. B*, 2005, **109**, 17192.
14 J. Spendelow, P. K. Babu and A. Wieckowski, *Curr. Opin. Solid State Mater. Sci.*, 2005, **9**, 37.
15 Y. Y. Tong, A. Wieckowski and E. Oldfield, *J. Phys. Chem. B*, 2002, **106**, 2434.
16 P. K. Babu, E. Oldfield and A. Wieckowski, in *Modern Aspects of Electrochemistry*, ed. C. Vayenas, B. E. Conway and R. E. White, Kluwer Academic/Plenum Publishers, New York, 2003, p. 1.
17 P. Waszczuk, J. Solla-Gullon, H. S. Kim, Y. Y. Tong, V. Montiel, A. Aldaz and A. Wieckowski, *J. Catal.*, 2001, **203**, 1.
18 P. K. Babu, H. S. Kim, E. Oldfield and A. Wieckowski, *J. Phys. Chem. B*, 2003, **107**, 7595.
19 H. T. Stokes, H. E. Rhodes, P. K. Wang, C. P. Slichter and J. H. Sinfelt, *Phys. Rev. B*, 1982, **26**, 3575.
20 H. E. Rhodes, P. K. Wang, H. T. Stokes, C. P. Slichter and J. H. Sinfelt, *Phys. Rev. B*, 1982, **27**, 3559.
21 J. J. van der Klink, *Adv. Catal.*, 2000, 1.
22 Y. Y. Tong, E. Oldfield and A. Wieckowski, *Anal. Chem.*, 1998, **70**, 518A.
23 J. P. Bucher and J. J. van der Klink, *Phys. Rev. B*, 1998, **38**, 11038.
24 C. P. Slichter, *Annu. Rev. Phys. Chem.*, 1986, **37**, 25.
25 T. Kobayashi, P. K. Babu, L. Gancs, J. H. Chung, E. Oldfield and A. Wieckowski, *J. Am. Chem. Soc.*, 2005, **127**, 14164.
26 C. P. Slichter, in *Principles of Magnetic Resonance*, Springer-Verlag, New York, 2nd edn, 1980.
27 N. Wakabayashi, M. Takeichi, M. Itagaki, H. Uchida and M. Watanabe, *J. Electroanal. Chem.*, 2005, **574**, 339.
28 N. Wakabayashi, M. Takeichi, H. Uchida and M. Watanabe, *J. Phys. Chem. B*, 2005, **109**, 5836.
29 H. Yano, E. Higuchi, H. Uchida and M. Watanabe, *J. Phys. Chem. B*, 2006, **110**, 16549.
30 E. Higuchi, H. Uchida and M. Watanabe, *J. Electroanal. Chem.*, 2005, **583**, 69.
31 Y. Y. Tong, C. Belrose, A. Wieckowski and E. Oldfield, *J. Am. Chem. Soc.*, 1997, **119**, 11709.
32 S. K. Zecevic, J. S. Wainright, M. H. Litt, S. L. Gojkovic and R. F. Savinell, *J. Electrochem. Soc.*, 1997, **144**, 2973.
33 D. R. Lawson, L. D. Whiteley and C. R. Martin, *J. Electrochem. Soc.*, 1988, **135**, 2247.
34 D. Chu, D. Tryk, D. Gervasio and E. B. Yeager, *J. Electroanal. Chem.*, 1989, **272**, 277.
35 D. Chu, *Electrochim. Acta*, 1998, **43**, 3711.
36 Y. Ayato, K. Kunimatsu, M. Osawa and T. Okada, *J. Electrochem. Soc.*, 2006, **153**, A203.
37 N. Markovic, H. Gasteiger and P. N. Ross, *J. Electrochem. Soc.*, 1997, **144**, 1591.
38 Y. Yafet and V. Jaccarino, *Phys. Rev.*, 1964, **133**, A1630.
39 M. Weinert and A. J. Freeman, *Phys. Rev. B*, 1983, **28**, 6262.
40 J. P. Bucher, J. Buttet, J. J. van der Klink and M. Graetzel, *Surf. Sci.*, 1989, **214**, 347.
41 J. J. van der Klink, *J. Phys.: Condens. Matter*, 1996, **8**, 1845.
42 Y. Y. Tong, C. Rice, N. Godbout, A. Wieckowski and E. Oldfield, *J. Am. Chem. Soc.*, 1999, **121**, 2996.
43 C. Rice, Y. Y. Tong, E. Oldfield and A. Wieckowski, *Electrochim. Acta*, 1998, **43**, 2825.
44 P. A. Vuissoz, J. P. Ansermet and A. Wieckowski, *Electrochim. Acta*, 1998, **44**, 397.